ISSN 1070-3632, Russian Journal of General Chemistry, 2013, Vol. 83, No. 1, pp. 1–9. © Pleiades Publishing, Ltd., 2013.
Original Russian Text © V.V. Bakovets, L.N. Trushnikova, I.V. Korol'kov, P.E. Plyusnin, I.P. Dolgovesova, T.D. Pivovarova, N.I. Alferova, 2013, published in Zhurnal Obshchei Khimii, 2013, Vol. 83, No. 1, pp. 3–12.

Synthesis of the Nanostructured Luminophor Y_2O_3–Eu–Bi by the Sol–Gel Method

V. V. Bakovets, L. N. Trushnikova, I. V. Korol'kov, P. E. Plyusnin, I. P. Dolgovesova, T. D. Pivovarova, and N. I. Alferova

Nikolaev Institute of Inorganic Chemistry, Siberian Division, Russian Academy of Sciences, pr. Akademika Lebedeva 3, Novosibirsk, 630090 Russia
e-mail: becamde@niic.nsc.ru

Received June 30, 2011

Abstract—The sol-gel method of the formation of the nanostructured luminophor based on Y_2O_3 doped by Eu^{3+} and Bi^{3+} was studied. The mechanism of the dehydration and dehydroxylation of gels and xerogels of the mixed hydroxides, particle sizes, structure, and luminescent properties of the synthesized products based on Y_2O_3 depend on the chemical nature of a precipitating agent (NaOH or NH_4OH) and a washing agent (water and alcohol).

DOI: 10.1134/S1070363213010015

Development of modern microdisplays requires luminescent nanostructured materials to be created with the particle size distribution as close to monodisperse as possible [1–5]. A luminophor based on yttrium oxide and doped by 4–5 mol % of europium is well-known as a source of the emission spectrum red component [1-8]. Wide application of this luminophor in cathode ray tubes, displays, and various luminescent devices alongside with its high thermal and chemical stability attracts attention of researchers and industrial engineers to the optimization of optical properties of this material. To improve the effectiveness of luminophors based on oxides of rare earth elements, ions of coactivators are added to them. Such a coactivator is, for example, bismuth, as its ions increase the effectiveness of radiation of europium ions. Activation of Y_2O_3–Eu, Gd_2O_3–Eu, and La_2O_3–Eu oxides by Bi^{3+} ions was studied in [9, 10]. Yttrium, gadolinium, and lanthanum oxides form solid solutions with Bi_2O_3 owing to closeness of ionic radii of the metals: $r(Bi^{3+})$ 0.96, $r(Y^{3+})$ 0.92, $r(Gd^{3+})$ 0.97, and $r(La^{3+})$ 1.14 Å. Of these three active matrices, Y_2O_3 oxide is the most effective for the activation of radiation by Bi^{3+} ions.

The application of luminophors based on oxides of rare earth elements involves an increase in the cost of the material and thus a problem arises of the minimization of applied amounts of rare earth elements provided that the luminophor effectiveness is retained. This problem can be solved by decreasing luminophor particle sizes to a minimal limit, down to nanometer range, at which the radiation intensity remains close to the intensity of a macrocrystalline luminophor [11, 12].

One of the most comprehensible methods of the synthesis of nanostructured materials, for example metal oxides, is the sol-gel method [13]. This method was used for the synthesis of yttrium oxide doped with europium and bismuth, Y_2O_3–Eu, Bi, by the co-precipitation of metal hydroxides, carbonates, or oxalates [1, 9], but in these and other works the problem of the formation of nanostructured material was not considered. At the same time it was shown that the coprecipitation of hydroxides by the sol-gel method yields a luminophor with enhanced luminescence intensity as compared to a luminophor of the same composition prepared by a solid-phase caking of Y, Eu, and Bi oxides and salts [10]. The most effective luminophors were obtained by the precipitation of hydroxides based on the specified compositions under hydrothermal conditions, which results in the formation of micron-size crystals. During the subsequent dehydration at elevated temperatures of hydrogel formed in the intermediate stage the particles are caking together, and their sizes essentially increase. It is obvious that the control over particle sizes requires a detailed study of dehydration processes and

the formation of a microstructure, for example of coprecipitated Y, Eu, and Bi hydroxides. The synthesis of nanostructured composites by the sol–gel method has some special features: sol precipitation by an alkali metal hydroxide or by ammonia, washing the obtained precipitate by water or alcohols, and variation of dehydration regimes of the resulting hydrogels. The influence of these features of the synthesis on the dehydration mechanism and particle sizes was not studied in detail.

The aim of this work was to study the mechanism of dehydration of yttrium hydroxide and products of its coprecipitation with europium and bismuth hydroxides to corresponding oxides and their solid solutions using the specified variations of process conditions and to study the effect of these variations on the microstructure of formed powders.

Yttrium oxide – precipitation by NaOH (series I). Generally the formation of oxides of rare earth elements can be described by stages of the thermal decomposition of hydrogels of their hydroxides [Eqs. (1)–(3)].

$$Ln(OH)_3 \cdot nH_2O = Ln(OH)_3 + nH_2O\uparrow, \quad (1)$$

$$Ln(OH)_3 = LnO(OH) + H_2O\uparrow, \quad (2)$$

$$2LnO(OH) = 2Ln_2O_3 + H_2O\uparrow. \quad (3)$$

Thermal action in each stage defines sizes of formed crystal grains and particles. When the processes are carried out under hydrothermal conditions, these stages are clearly separated [14, 15], and particles of thus obtained materials are of size lying within the micrometer range. When particles with nanometer sizes are formed under normal pressures, the specified stages are not always clearly pronounced, and the understanding of the process mechanism requires detailed and comprehensive study.

The results of the thermal analysis of dehydration and dehydroxylation of the $Y(OH)_3 \cdot nH_2O$ hydrogel carried out in an 1:4 oxygen-argon mixture are presented in Fig. 1. The weight loss curve for samples of series I (Fig. 1a) has no sharply expressed curvature changes, and only the derivative of this curve allows us to distinguish a great number of distinct stages of the product thermal conversion. The appearance of an exothermic peak at 650°C and a simultaneous acceleration of the weight loss connected with the sample dehydroxylation are rather common. It is usually attributed to a dominance of an exothermic crystallization effect over an endothermic dehydroxylation effect [16]. Figure 2a shows the dependence of the weight loss of samples obtained by the sol-gel precipitation on the temperature of their annealing within 2 h. The monotone decrease in the sample weight is observed. Diffractograms of the products of annealing samples of series I up to 500°C are presented in Fig. 3a (curves *1*–*7*). The samples are amorphous and partially nanocrystalline. The disposition of observed single diffusion reflexes suggests that the nanostructured microdomains of $Y(OH)_3$, YO(OH), $YOHCO_3$, $Y_2(CO_3)_3$, and Y_2O_3 are present. At 600°C almost pure cubic Y_2O_3 (PDF no. 41-1105) [17] is present, which becomes polycrystalline at 1200°C. The data of the phase analysis of products of the sol-gel synthesis and of their subsequent dehydration and dehydroxylation are presented in the table together with the coherent scattering regions (CSR) for the basic crystal planes.

The IR spectra of samples after annealing at fixed temperatures are presented in Fig. 4. Absorption bands in the range of wave numbers less than 500 cm^{-1} refer to Y–O bonds [18] and are observed for samples annealed at temperatures higher than 600°C. The wide band with a maximum at 3500 cm^{-1} corresponds to the superposition of bands of single OH groups in H_2O and $YOHCO_3$ molecules [19]. For samples of series I (Fig. 4a) absorption bands at 1700, 1530, 1400, 1100, and 850 cm^{-1} corrspond to C–O bonds in CO_2 and CO_3^{2-} [15, 19, 20]. A series of bands at 850, 1050, and 1390 cm^{-1} is assignable to N–O bonds [21, 22]. The detailed analysis of the IR spectrum of $Y(NO_3)_3 \cdot 4H_2O$ has shown [23] that the band at 1390 cm^{-1} is forbidden for this compound. The chemical analysis by the capillary electrophoresis method has shown that nitrate ions at a level from 0.03 up to 0.05 wt % are present in a sample annealed at 500°C. Therefore, the IR spectra of the precipitated products after annealing can be assigned to a mixture of yttrium hydroxides and hydrocarbonates. These latter are formed during the sol-gel synthesis in air medium, which is characteristic for aqueous solutions of rare earth elements [24]. The presence of nitrate ions and the scatter of their amounts from one sample to another are connected with incomplete washing out a gel precipitate, which was carried out at periodic intermixing in a Buchner funnel.

Thus, the combination of the thermal analysis, diffractometry, and IR spectroscopy data allows us the characterization of the annealing process of series I samples by the superposition of a great number of sequential and parallel stages of yttrium trihydroxide

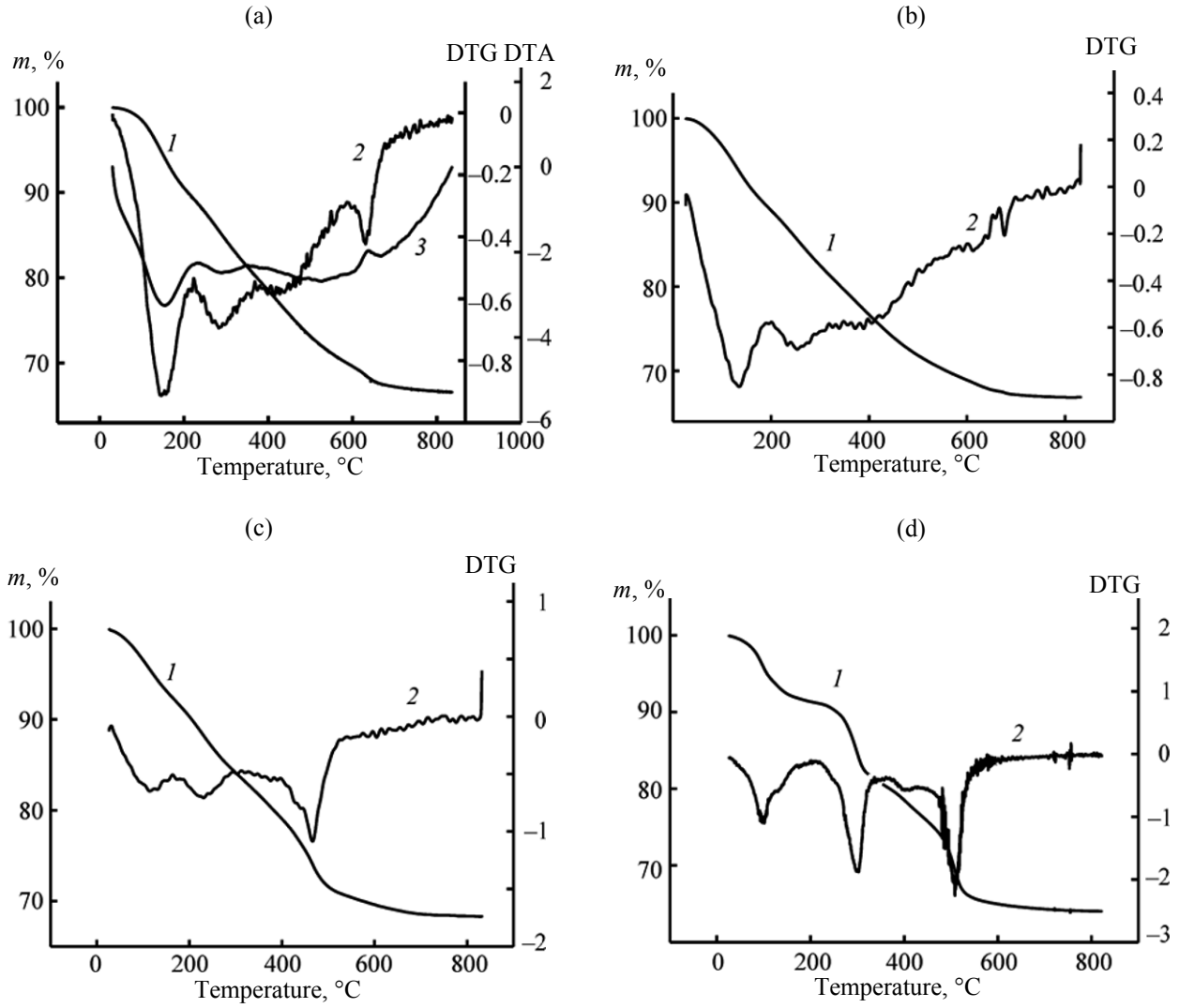

Fig. 1. Thermal analysis of samples after drying at 50°C. Series: (a) **I**, (b) **II**, (c) **III**, and (d) **IV**. Curves: (*1*) TG, (*2*) DTG, (*3*) DTA.

dehydroxylation, which were also found in [14, 25], and by the decomposition of intermediate yttrium hydrocarbonates described in [26]. It causes a monotonic run of the weight loss curve with increasing temperature. Probably, all the mentioned processes are connected with structural transformations resulting in hampering Y_2O_3 crystallization up to 600–700°C.

Temperature dependences of specific surface area S, pycnometric specific gravity ρ, and average particle size D calculated by the equation $D = 6/S_{sp}/\rho$ for samples of series I, III, and IV, respectively are presented in Figs. 2b–2d. These dependences are also monotonic for samples of series I, except for a small reproducible deviation from monotonicity in the regions of 220 and 500–600°C. These deviations occur frequently in hydroxides of other metals obtained by the sol–gel method [27], which is due to the fact that the dehydration stage is transformed to the dehydroxylation stage with the formation and crystallization of a xerogel. The average particle size reaches 15 nm at the annealing temperature of 600°C and 40–60 nm at 1200°C for samples of series I.

The nanostructured film formed from Y_2O_3 particles synthesized on the silicon substrate surface is shown in Fig. 5. Its particle size is close to the size found by the above-stated equation. As follows from the comparison of the data of the table and Fig. 2d, the size of crystal grains actually coincides with the particle size.

Yttrium oxide doped by luminescent activators - precipitation by NaOH (series II and III). Precipitation products, which are red luminophor

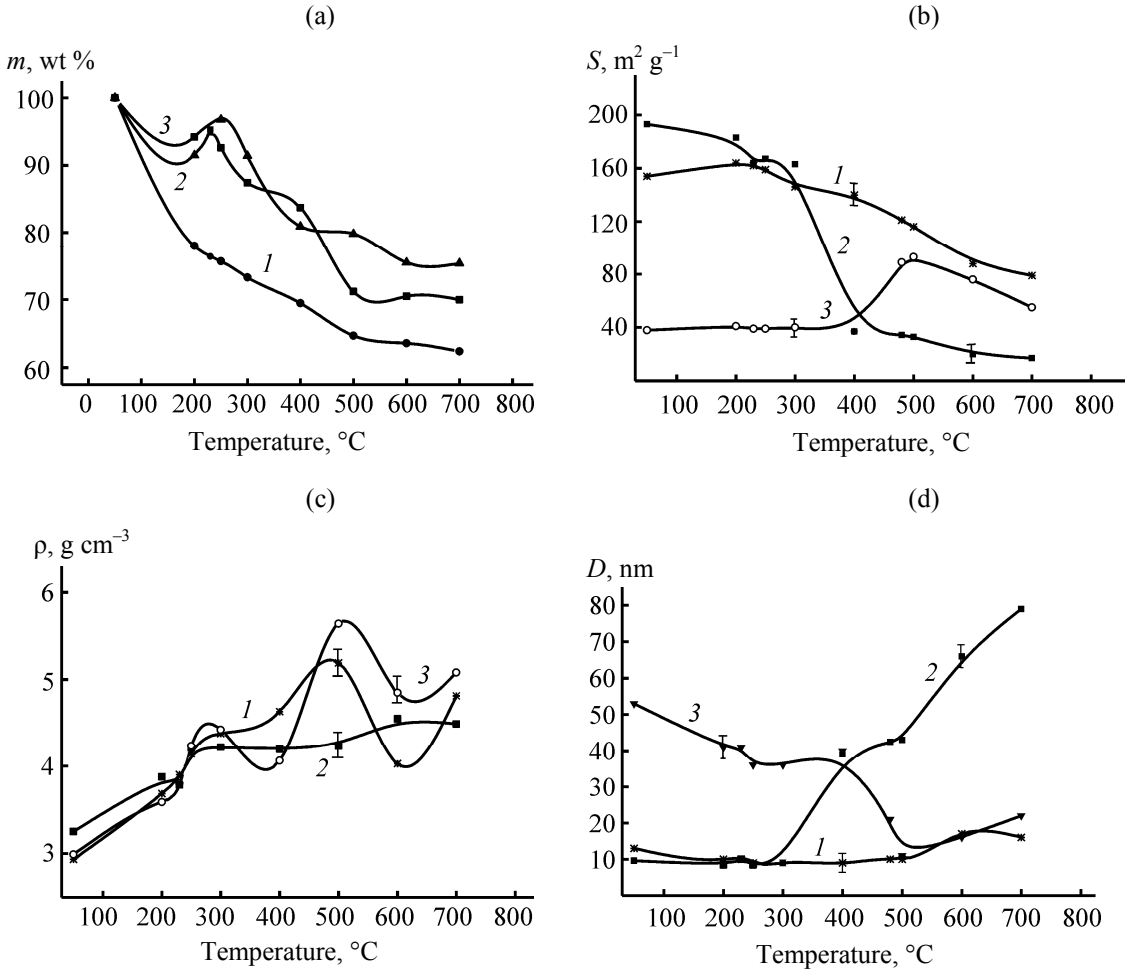

Fig. 2. Variation of parameters of samples with increasing annealing temperature. (a) Weight loss, (b) specific surface area, (c) pycnometric specific gravity, and (d) average particle sizes. Sample series: (*1*) **I**, (*2*) **III**, and (*3*) **IV**.

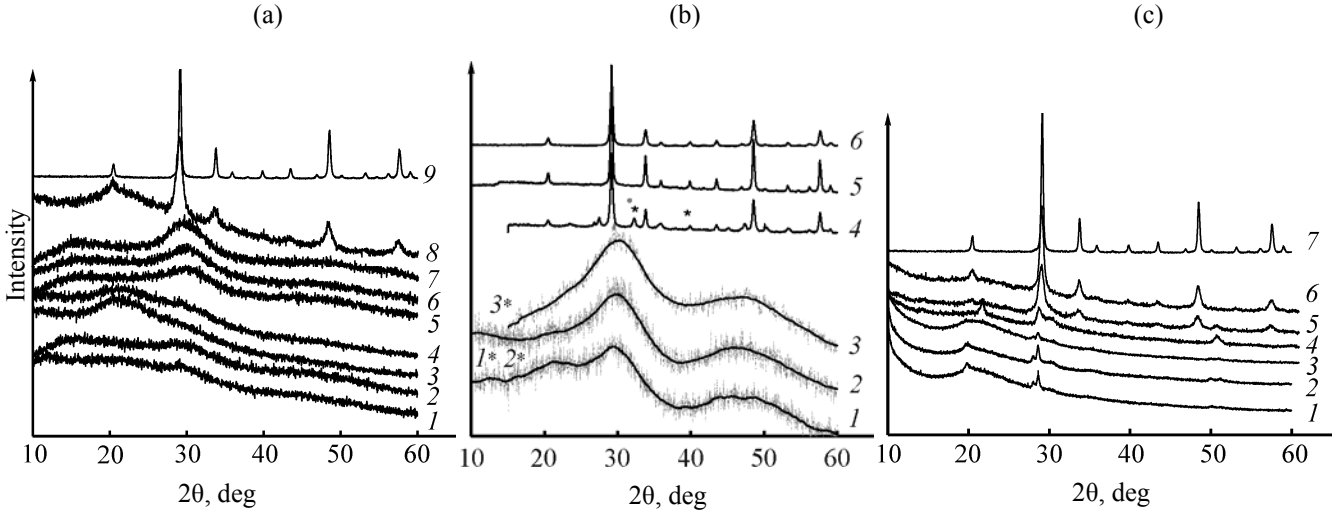

Fig. 3. Diffractograms of samples. (a) Series I after annealing at temperatures, °C: (*1*) 50, (*2*) 200, (*3*) 230, (*4*) 250, (*5*) 300, (*6*) 400, (*7*) 500, (*8*) 600, (*9*) 1200; (b) series III after annealing at temperatures, °C: (*1*) 200, (*2*) 230, (*3*) 300, (*4*) 500, (*5*) 700, (*6*) 1200; (c) series IV after annealing at temperatures, °C: (*1*) 200, (*2*) 230, (*3*) 250, (*4*) 400, (*5*) 500, (*6*) 700, (*7*) 1200.

Phase analysis data

Sample, T_{anneal}, °C	Composition	CSR, nm		
		(222)	(004)	(044)
Pure Y_2O_3[a] (series I)				
50–500	Amorph	–	–	–
600	Y_2O_3	15(2)	13(2)	13(2)
1200	Y_2O_3	43(9)	43(9)	61
Y_2O_3–Eu-Bi[b] (series III)				
50	Amorph	–	–	–
200–300	Amorph + $NaBiO_3$ + Na_3BiO_4	–	–	–
300	Amorph	–	–	–
500	Y_2O_3 + un. ph.	42(8)	55(9)	65(9)
700	Y_2O_3	92(15)	98(15)	150(40)
1200	Y_2O_3	600–700	600–700	600–700
Y_2O_3–Eu-Bi[c] (series IV)				
200–250	Amorph + un. ph.	–	–	–
400	un. ph.	–	–	–
500	Y_2O_3 + un. ph.	17(3)	12(2)	16(3)
700	Y_2O_3	25(3)	22(3)	24(3)
1200	Y_2O_3	63(10)	62(10)	81(15)

[a] Precipitation with NaOH, washing with water. [b] Precipitation with NaOH, washing with alcohol. [c] Precipitation with NH_4OH, washing with water. (un. ph) unknown phases, (CSR) coherent scattering regions.

precursors, represent a mechanical mixture and solid solutions of hydrogels of the oxides Y_2O_3, Eu_2O_3 (5 mol %) and Bi_2O_3 (0.5 mol %). The study of the formation of the doped yttrium oxide by the sol-gel method has shown that when the hydrogel is washed with water (series II), regularities of annealing are almost identical to those found earlier for not doped yttrium oxide (series I). Appreciable changes are observed when the precipitated hydrogel is washed with alcohols (isopropanol, series III). Thermograms of the corresponding precipitation products prepared in an oxygen-argon mixture are presented in Figs. 1b and 1c.

It is seen from the presented data that Fig. 1b is similar to Fig. 1a. It means that the dehydration and dehydroxylation of non-doped yttrium hydroxide (series I) and of that doped by europium and bismuth and washed with water (series II) follow the same mechanism. Washing of the precipitation product by alcohol results in a change of the dehydration and dehydroxylation mechanism. The dehydration of the sample washed with alcohol at 100°C (Fig. 1c) is less pronounced, whereas the two-stage weight loss occurs in the temperature range 400–500°C, and no intensive weight loss takes place in the range 600–700°C.

Dependences of weight loss of series II samples on the temperature of product annealing in a furnace differ from those for non-doped samples (series I) only slightly. The weight loss for series III samples washed with alcohol is much less (Fig. 1c), and its temperature dependence has anomalies at 200-250 and 400–500°C. The diffractometry data (Fig. 3b) show that the formation of crystalline yttrium oxide in series III samples occurs between 300 and 400°C. It is lower by 200–300°C than the crystallization temperature of samples washed with water. In the range of 200-300°C the sample is close to amorphous, and the observed stucturization can be assigned to main reflexes of $NaBiO_3$ and Na_3BiO_4 (PDF nos. 1-90, 27-654, and 71-1583) [17]. At 300°C the main reflexes of yttrium oxide in the form of wide peaks are clearly seen, the crystalline hydrocarbonate $YOHCO_3$ (PDF nos. 30-1444, 32-1429, and 70-278) being formed alongside with yttrium oxide [17]. As the annealing temperature increases (400–500°C), the absorption at 860 and 1500 cm^{-1} in the IR spectra of the samples increases (Fig. 4b), which corresponds to the formation of hydro- and anhydrous carbonates [26]. As the annealing temperature increases further, this phase disappears also from the diffractograms, in the IR spectra yttrium oxide is detected, and after 400°C also lowest yttrium carbonates are found, which are almost completely decomposed at 1200°C. The weight loss in the range of 400–500°C is probably connected with

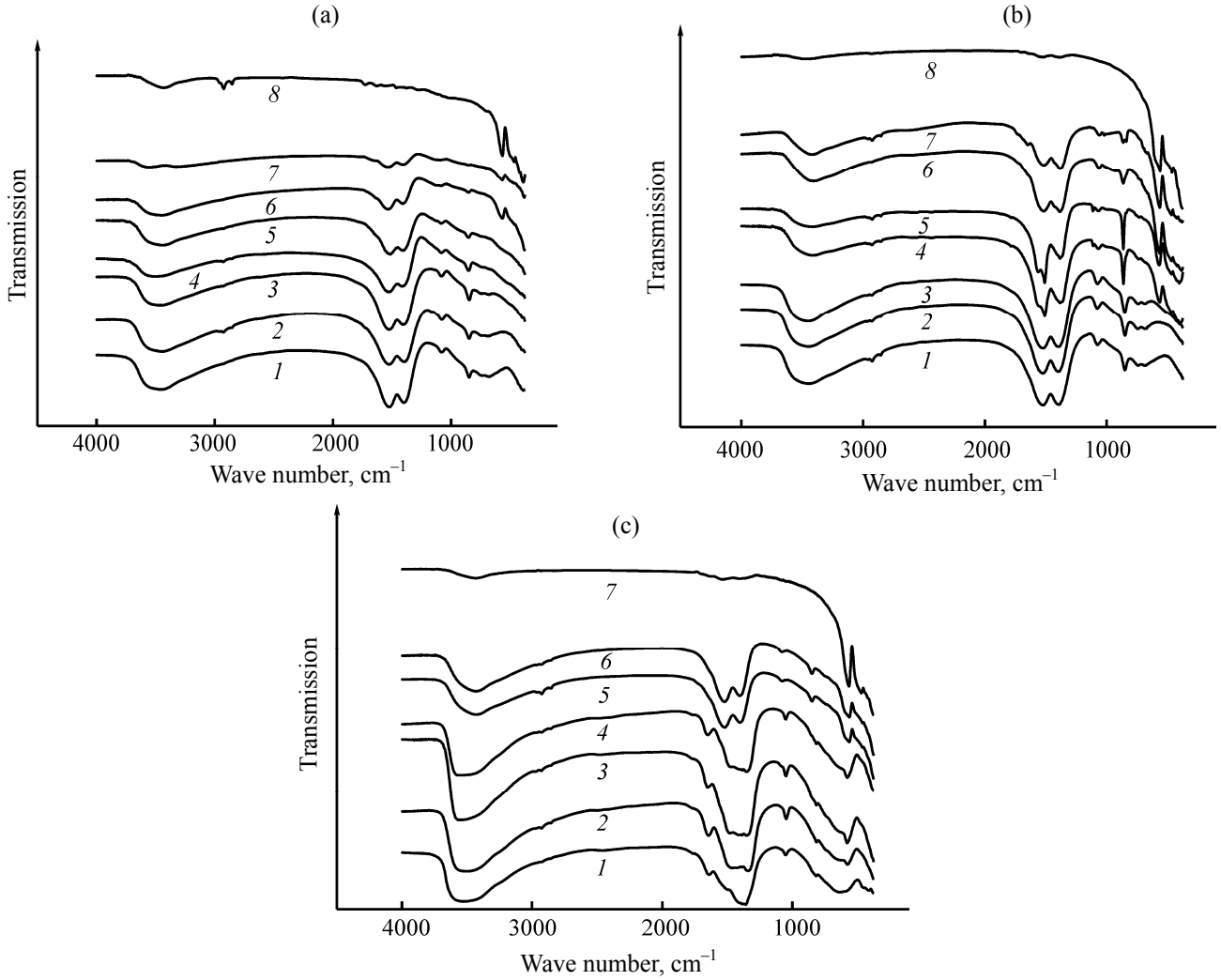

Fig. 4. IR spectra of products of annealing samples of (a) series I at temperatures, °C: (*1*) 200, (*2*) 230, (*3*) 300, (*4*) 400, (*5*) 500, (*6*) 600, (*7*) 700, (*8*) 1200; (b) series III at: (*1*) 200, (*2*) 230, (*3*) 300, (*4*) 400, (*5*) 500, (*6*) 600, (*7*) 700, (*8*) 1200; (c) series IV at: (*1*) 230, (*2*) 300, (*3*) 400, (*4*) 500, (*5*) 600, (6) 700, (*7*) 1200.

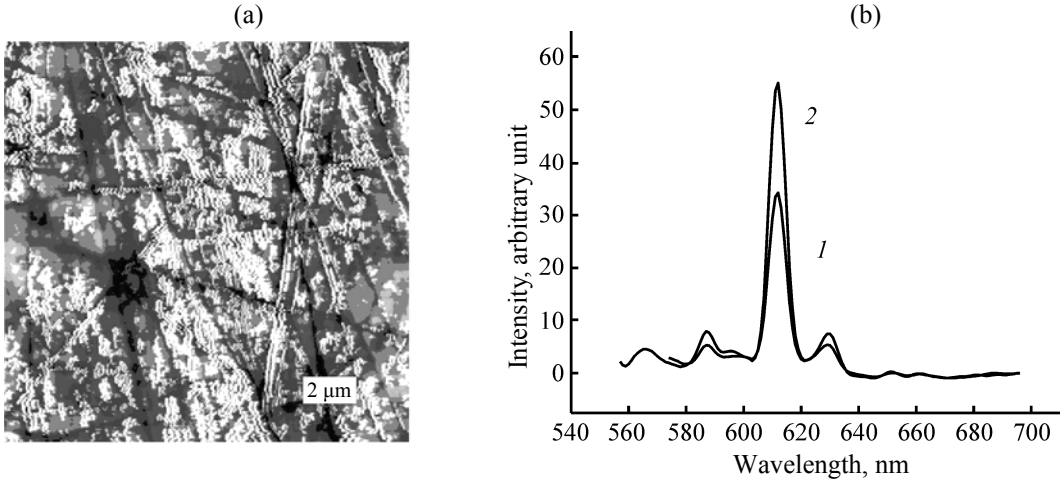

Fig. 5. (a) Nanostructured film of 15–20 nm particles of series I sample annealed at 600°C. A photo obtained using atomic-force microscopy. (b) Luminescent spectra of series IV samples, excitation on the wave length of 225 nm, annealing at (*1*) 700, (*2*) 1200°C.

vaporization of products of isopropanol decomposition, as it was observed in the case of nickel alcogel decomposition [27]. Furthermore, in the case of yttrium hydroxide precipitated in the sol-gel process, the washing with isopropanol considerably dehydrates the gel, which results in the effects of the low-temperature decomposition of neutral carbonates [26]. Curves *2* in Figs. 2b-2d represent variations of specific surface area *S*, pycnometric specific gravity ρ, and average particle size *D* of the samples, respectively. These data point to increased dispersity and porosity of precipitation products of series III samples after drying at 50°C, which can be related to increasing probability of the formation of a significant amount of yttrium alcogels [28] with much more loose microstructure than that of hydrogels. The polycondensation with alcohol splitting occurs at low temperatures faster than the dehydroxylation, which results in a sharp decrease in *S* with increasing temperature, and in the increase in the xerogel density and in the size of yttrium oxide particles up to 80 nm. The temperature dependences under consideration also have anomalies at 250 and 500°C. In connection with the fact that the oxide crystallization begins at low temperatures, the size of crystal grains at 500°C is 2–4 times larger than that of non-doped samples washed with water, and reaches 50 nm on the average. Sizes of crystal grains practically coincide with particle sizes (Fig. 2d, curve 2, see the table). The annealing of the samples at 700 and 1200°C results in the size increase up to 90 and 600 nm, respectively.

Yttrium oxide doped by luminescent activators-precipitation by NH_4OH (series IV). The thermogram of a hydrogel of yttrium, europium, and bismuth hydroxides precipitated by an NH_4OH solution and washed with water is presented in Fig. 1d. Unlike samples presented earlier, the weight loss exhibits a clearly pronounced staging as the temperature increases. It is known that stable ammines of nitrates of lanthanides $Ln(NO_3)_3 \cdot nNH_3$ [21] are formed in systems with ammonia and nitrates of lanthanides, and in air double carbonates $NH_4[Ln(CO_3)_2] \cdot nNH_3$ are also formed [26].

Diffractograms of samples annealed at various temperatures in a furnace (Fig. 3c) show that a crystal phase appears even at 200°C. The IR spectra of samples annealed at various temperatures are presented in Fig. 4c. Unlike samples of series I and III, in the IR spectra of series IV samples there are additional absorption bands at 1646, 1410, and 620 cm^{-1} and the band enhancement in the short-wave range is observed. These bands disappear after annealing at 500°C. The specified bands have been identified earlier in ammines of nitrates [17]. The combination of the presented data points to the existence of intermediate compounds containing NH_4^+ cations in hydrogel, which are removed on heating above 500°C, as it was recorded in the DTG curve of the diffractogram at 300 and 500°C (Fig. 3c, curve *4*). Above this temperature the diffractograms (see the table) and the IR spectra of samples correspond to yttrium oxide with traces of yttrium carbonates [21], which are decomposed completely about 1200°C.

It follows from Figs. 2b–2d (curves *3*) that, in contrast to the previous series, series IV samples in the hydrogel and xerogel states have a rather small *S* value, and on the dehydroxylation in the temperature range 500–600°C particle sizes of oxide become identical to sizes of series I samples. The density of samples varies similarly to that of the sample precipitated by the NaOH solution. In the region of 500°C *S* value increases more than twice, and the particle size decreases in the same ratio up to the values corresponding to the above-described samples. The size of crystal grains practically coincides with the size of nanoparticles (see the table).

Luminescent properties of the obtained samples. Of the synthesized samples, only samples doped with a red radiation activator Eu^{3+} and a Bi^{3+} coactivator show luminescent properties, namely the samples, which were precipitated by the ammonium hydroxide solution. Samples precipitated by a NaOH solution did not show luminescence after annealing at 700°C and even at 1200°C. Quenching of the Eu^{3+} radiation in the case of these samples can be connected only with the formation of $NaBiO_3$ and Na_3BiO_4, which were detected by the X-ray method in the samples annealed at low temperatures. Repeated experiments with precipitation of hydroxides by the NaOH solution in the absence of Bi always gave rise to the characteristic Eu^{3+} luminescence. As it was found by the flame photometry method, in presence of Bi sodium is washed off only up to 0.02 wt %. No Na admixture was found after washing samples free from Bi.

After annealing series III samples at 1200°C the samples become yellow-brownish, which is characteristic for isolated free phases of bismuth oxides. Low-intensive reflexes appear simultaneously in diffractograms of the samples (Fig. 3b), which are close in

position to $NaY_{0.95}Eu_{0.05}O_2$ peaks (PDF no. 20-1179 [17]). Probably the isolation of a separate phase of bismuth oxide also results in quenching the Eu^{3+} radiation. Except for that a sharp enlargement of crystal grains up to 500 nm and more is observed, which points to acceleration of crystal grains growth. Photoluminescence spectra of samples of the $Y_{1.87}Eu_{0.12}\cdot Bi_{0.01}O_3$ solid solution (series IV) are presented in Fig. 5. It is seen that the increase in annealing temperature up to 1200°C results in a raise of intensity of the emission band at 611.7 nm.

Thus, the use of the sol–gel method for the formation of nanostructured luminophor based on Y_2O_3 and doped by Eu^{3+} and Bi^{3+} activators in optimal concentrations of 4.3 and 0.5 mol %, respectively, has shown that the mechanism of formation, structure, and luminescent properties of the resulting samples depend on the chemical nature of the agent precipitating a mixture of Y, Eu, and Bi hydroxides, and also on the synthesis pathway through a hydrogel or an alcogel. The precipitation of the hydroxides by NaOH with the use of a Bi^3+ luminescence result in the formation of sodium bismuthates, which provoke quenching Eu^{3+} luminescence. The long-term washing of a precipitate of hydroxides with alcohols results in the formation of alcogels, which promotes the formation of microporous alcogels with a specific surface area as high as 200 $m^2\ g^{-1}$, however particle sizes of yttrium hydroxide increase by factors of 4 and 10 after annealing at 700 and 1200°C as compared to the samples washed with water, and reach 90 and 600 nm, respectively. Average particle sizes for all considered series of samples practically coincide with average sizes of crystal grains. The Y_2O_3-Eu-Bi luminophors precipitated by ammonia have rather small particles (25 and 60 nm for samples annealed at 700 and 1200°C, respectively). Intensity of Eu^{3+} luminescence in these samples increases as annealing temperature increases. The limited increase in the average particle size in this case is connected probably with sequential structural transformations of ammines of nitrates and yttrium hydrocarbonates, and with their decomposition. The results obtained allow us to recommend the sol–gel method for the formation of nanostructured lumine-scent materials, and at that the optimization of particle sizes of the most intensive luminophor can be reached by increasing temperature and time of annealing.

EXPERIMENTAL

We used in the work yttrium and europium nitrates $Y(NO_3)_3\cdot 6H_2O$ and $Eu(NO_3)_3\cdot 5H_2O$ prepared from corresponding oxides and containing no less than 99.9% of main components, Bi_2O_3 (special-purity grade), precipitating agents NH_4OH (special-purity grade) and NaOH (analytical grade), and isopropanol (special-purity grade). Contents of activators in yttrium oxide were assumed to be 4.3 mol % of Eu and 0.5 mol % of Bi. To obtain yttrium hydroxides, a 0.2 M solution of yttrium nitrate was prepared. Doping by europium and bismuth was carried out by adding to a solution required amounts of europium nitrate and bismuth oxide dissolved beforehand in diluted (1:1) nitric acid. Volume of the solution was brought up to 320 ml by distilled water, and then 50 ml of isopropanol was added to it. A 2.6 M NH_4OH solution was prepared by dilution of 21 ml of concentrated ammonia by 355 ml of distilled water (version 1). It corresponded to a triple excess as compared to the precipitation reaction stoichometry ($[Y^{3+}]/[NH_4^+] = 1/3$). In version 2 a 1.44 M NaOH solution (twofold excess) was used as a precipitating agent. Solutions of the initial nitrates and a precipitating agent were placed in separate separatory funnels, from which they were fed in a two-liter set up equipped with a heating mantle and containing 300 ml of water. During the synthesis pH of the solution was kept constant at 12.5. After reaching water temperature of ~70°C solutions were fed simultaneously into the flask by spraying with compressed air preheated in a thermostat up to 70°C [29]. After termination of the precipitation the mixing was continued for 30 min. Precipitated hydroxides were washed on a Buchner funnel with a great amount of water (about 2 l) up to a neutral reaction or with isopropanol. Samples washed out and separated on the filter from the mother liquor were dried at 50°C to a constant weight.

The following series of samples were prepared in such a way: pure yttrium oxide precipitated by sodium hydroxide and washed with water (series I); yttrium oxide doped with Eu (4.3 mol %) and Bi (0.5 mol %) precipitated by sodium hydroxide and washed with water (series II) and isopropanol (series III); yttrium oxide doped with Eu (4.3 mol %) and Bi (0.5 mol %) precipitated by ammonia and washed with water (series IV).

Samples, which have been dried at 50°C, were studied by the thermal analysis method using a NETZSCH TG 209 F1 microbalance (heating rate of 10 grad/min in the O_2–Ar mixture, 1:4). Further a gravimetric analysis was carried out with a thermal treatment at 230, 250, 300, 400, 500, 600, and 700°C

for 2 h in air. The specific surface area of samples S_{sp} was determined in each stage of annealing on a Sorbtometer-M adsorption analyzer with a relative standard deviation of 5%. A density of samples was determined by the pycnometer method with a relative error of 0.2-0.5%, using bidistilled water as a working liquid. The X-ray analysis of samples was carried out on a DRON-3M diffractometer (CuK_α radiation, Ni filter, range of 2θ angles from 10 up to 60°). Ranges of a coherent scattering were determined by the known Scherrer equation with silicon as the exterior measurement standard. Morphology of particles was controlled by the atomic force microscopy method. Contents of Na in samples precipitated by the NaOH solution were determined by the flame photometry method and contents of residual NO_3^- anions, by the capillary electrophoresis method.

REFERENCES

1. Zhang, J. and Hong, G.J., *J. Sol. State Chem*., 2004, vol. 177, no. 4, p. 1292.
2. Sun, L., Qian, C., Liao, C., Wang, X., and Yan, C., *Sol. State Commun*., 2001, vol. 119, no. 6, p. 393.
3. Liu, L., Peng, Q., and Li, Y., *Inorg. Chem*., 2008, vol. 47, no. 11, p. 5022.
4. Maestro, P. and Huguenin, D.J., *J. Alloys Comp*., 1995, vol. 225, no. 2, p. 520.
5. Bakhmet'ev, V.V., Korsakov, V.G., Mikhailova, E.V., Miakin, S.V., and Sychov, M.M., Abstracts of Papers, *XVIII Advanced Display Technologies International Symposium*, SID, St. Petersburg, 2010, p. 197.
6. Maestro, P., Huguenin, D., Seigneurin, A., Deneuve, F., Lann, P., and Berar, J.F., *J. Electrochem. Soc*., 1992, vol. 139, no. 5, p. 1479.
7. Wakefield, B.G., Holland, E., Dobson, P.I., and Hutchison, T.L., *Adv. Mater*., 2001, vol. 13, no. 20, p. 1557.
8. Kitai, A.H., *Thin Solid Films*, 2003, vol. 445, no. 2, p. 367.
9. Datta, R.K., *J. Electrochem. Soc*., 1967, vol. 114, no. 11, p. 1137.
10. Chi, L.S., Liu, R.S., and Lee, B.J., *J. Electrochem. Soc*., 2005, vol. 152, no. 8, p. J93.
11. Kang, Y.C., Lenggovo, I.W., Okuyama, K., and Park, S.B., *J. Electrochem. Soc*., 1999, vol. 146, no. 3, p. 1227.
12. Flores-Gonzales, M.A., Ledoux, G., Roux, S., Lebbou, K., Perriat, P., and Tillement, O., *J. Solid State Chem*., 2005, vol. 178, no. 4, p. 989.
13. Kwiatkowski, K.C. and Lukehart, C.M, *Nanocanocomposites Prepared by Sol-Gel Methods: Synthesis and Characterization of Nanostructured Materials and Nanotecnology*, San Diego, 2000.
14. Fricke, R. and Seitz, A., *Z. Anorg. Allg. Chem*., 1947, vol. 254, nos. 1–2, p. 107.
15. Dorman, J.A., Mao, Y., Bargar, J.R., and Chang, J.P., *J. Phys. Chem. (C),* 2010, vol. 114, no. 41, p. 17422.
16. Serebrennikov, V.V., *Khimiya redkozemel'nykh elementov* (Chemistry of Rare Earth Elements), Tomsk: TGU, 1959, vol. 1.
17. *Powder Diffraction File. Alphabetical Index. Inorganic Phases*, JCPDS, International Centre for Diffraction Data, Pennsylva-nia, USA, 1983.
18. Chien W.-C., Yu Y.-Y., Yang C.-C., *Mater. Design*., 2010, vol. 31, no. 4, p. 1737.
19. Zhang, Y., Gao, M., Han, K., Fang, Z., Yin, X., and Xu, Z., *J. Alloys Comp*., 2009, vol. 474, no. 2, p. 598.
20. Srinivasan, R., Yogamalar, R., and Bose, A.C., *Mat. Res. Bull*., 2010, vol. 45, no. 9, p. 1165.
21. Torgonskaya, T.I. and Zababukha, N.I., *Zh. Neorg. Khim*., 1981, vol. 26, no. 8, p. 2076.
22. Bellamy, L.J., *The Infra-Red Spectra of Complex Molecules*, New York: John Wiley, 1957.
23. Kharitonov, Yu.A. and Babievskaya, I.Z., *Dokl. Akad. Nauk SSSR*, 1966, vol. 168, no. 3, p. 615.
24. Aghazadeh, M., Nozad, A., Adelkhant, H., and Ghaeml, M., *J. Electrochem. Soc*., 2010, vol. 157, no. 10, p. D519.
25. Cotton, F.A. and Wilkinson, G., *Advanced Inorganic Chemistry, A comprehensive Text*, New York: Interscience, 1966, 2nd ed.
26. *Soedineniya redkozemel'nykh elementov. Karbonaty. Oksalaty. Nitraty. Titanaty. Ser. Khimiya Redkikh Elementov* (Compounds of Rare Earth Elements. Carbonates. Oxalates. Nitrates. Titanates. Series Chemistry of Rare Elements), Moscow: Nauka, 1984.
27. Bakovets, V.V., Savintseva, S.A., Trushnikova, L.N., Plyusnin, P.E., Dolgovesova, I.P., Pivovarova, T.D., and Korol'kov, I.V., *Zh. Obshch. Khim*., 2010, vol. 80, no. 6, p. 945.
28. Bochkarev, M.N., Kalinina, G.S., Zakharov, L.N., and Khorshev, S.Ya., *Organicheskie proizvodnye redkozemel'nykh elementov* (Organic Derivatives of Rare Earth Elements), Moscow: Nauka, 1989.
29. Bakovets, V.V., Trushnikova, L.N., Korol'kov, I.V., Sokolov, V.V., Dolgovesova, I.P., and Pivovarova, T.D., *Zh. Obshch. Khim*., 2009, vol. 79, no. 3, p. 366.